Compton effect

Rico Schmidt and Guido Falk von Rudorff (Group M4)

I Introduction

In general, there are multiple ways of interaction between radiation and matter. Some of them are discussed below, but the main focus of the experiment is the Compton effect, which consists of angular dependent scattering. The Compton effect was the second process proving the wave-particle duality and has been discovered in 1922.

Usually, the signal from the Compton effect is predominates the spectrum. Depending on the circumstances of the data acquisition, such as the resolution of the detector, some of the other processes may be needed in order to explain all visible features. Hence, this section will start with a rough overview of interaction processes between radiation and matter. Afterwards, the setup of the experiment will be presented. Finally, the coincidence stage, the detector and the relevant decay types are explained in more detail.

I.A Photoelectric effect

The photoelectric effect was the first interaction process to be discovered. If photons with an energy E_γ hit an electron with the binding energy $E_B \ll E_\gamma$, the electron will be detached from the nucleus due to the photoelectric effect and carries the kinetic energy E_m

$$E_m = E_\gamma - E_B = hf - E_B \tag{1}$$

E_B is typically in the order of a few electron volts. Although the energy E_m is less than E_γ, the recombination leads to a measurement of roughly the full energy. The position with a lower energy level E_l that has been left empty will be filled by an electron from a higher energy level E_h. This can be achieved by emission of radiation which leads to the so called K_α and K_β peaks in the spectrum at

$$E_\alpha = E_h - E_l \tag{2}$$

for different E_h. E_l corresponds to the ground state. Usually these states are degenerated, but the difference between the energy levels is far to small to be measured with the equipment used in this experiment. The second possibility is the emission of Auger electrons that carry the energy

$$E_{ag} = E_\alpha - E'_B - E_B \tag{3}$$

Due to the fact that the Auger process involves three electrons and two of which are leaving the atom, two binding energies E_B and E'_B have to be subtracted. Firstly, the incoming photon detaches one electron. The second electron switches the energy level to that of the first one and emits a photon that detaches a third electron. The first electron is usually in one of the lowermost states.

Assuming that only electrons from the K shell are involved in the photo effect, the dependence on the atomic number Z of the photoelectric effect's cross section σ_P can be estimated[1] to be

$$\sigma_P \propto \frac{Z^4}{E^3} \tag{4}$$

The exact value for the exponent depends on the energy of the radiation–in general, higher energy leads to a smaller cross section. However, there is one exception: if the energy of radiation is a little bit smaller than the binding energy of a shell, the cross section drops significantly. This peak is named after the shell being involved. According to [2], the binding energies for electrons with quantum number n can be estimated by

$$E_b = \frac{R_y}{n^2} \begin{cases} (Z-1)^2 & n=1 \\ (Z-5)^2 & n=2 \\ (Z-13)^2 & n=3 \end{cases} \tag{5}$$

I.B Compton effect

The Compton effect is possible interaction of gamma rays with matter which shows pretty distinct features in the spectrum. As shown in Figure 1, any incident photon will be scattered by an angle φ while the electron gains some kinetic energy from the photon and changes its direction. Due to energy conservation, the wavelength of the photon increases. The amount of energy T transferred from the photon to the electron depends on φ.

$$T = E_\gamma \left(1 - \frac{1}{1 + \frac{E_\gamma}{m_e c^2}(1-\cos\varphi)}\right) \tag{6}$$

where E_γ is the energy of the photon before scattering. This formula can be obtained from the result of combining energy conservation

$$hf + m_0c^2 = hf' + mc^2 \tag{7}$$

$$\Leftrightarrow \quad m^2c^4 = h^2f^2 + h^2f'^2 + m_0^2c^4 - 2h^2f'f + 2hfm_0c^2 - 2m_0c^2hf' \tag{8}$$

Table I. Relevant constants.

symbol	value	comment
R_y	13.605 eV	universal
λ_C	2426 nm	electron only

and momentum conservation

$$\mathbf{p}_\gamma = \mathbf{p}'_\gamma + m_0\mathbf{v} \tag{9}$$

$$\Rightarrow m_0^2 v^2 = \frac{h^2 f^2}{c^2} - \frac{h^2 f'^2}{c^2} - 2\frac{h^2 f f'}{c^2}\cos\varphi \tag{10}$$

Starting from the relativistic expression for energy

$$E^2 - p^2c^2 = m^2c^4 \tag{11}$$

we get

$$2h^2 f f'(\cos\varphi - 1) - 2m_0c^2 h f' = -2hfm_0c^2 \tag{12}$$

and an expression for the new photon frequency

$$f' = \frac{f}{\frac{E_\gamma}{m_0c^2}(1-\cos\varphi)+1} \tag{13}$$

which in turn leads to

$$\lambda'_\gamma - \lambda_\gamma = \frac{h}{m_e c}(1-\cos\varphi) := \lambda_C(1-\cos\varphi) \tag{14}$$

where λ_C is the Compton wavelength. The Compton edge in Figure 3 results from the maximum energy $T_{\max}$ for $\varphi = \pi$

$$T_{\max} = E_\gamma\left(1 - \frac{1}{1+\frac{2E_\gamma}{m_0c^2}}\right) \tag{15}$$

The full spectrum can be derived[1] from the Klein-Nishina formula

$$\frac{\mathrm{d}\sigma}{\mathrm{d}\Omega} = \frac{1}{2}r_e^2 P(E,\varphi)\left(1 - P(E,\varphi)\sin^2\varphi + P(E,\varphi)^2\right) \tag{16}$$

$$P(E,\varphi) = \frac{1}{1+\varepsilon(1-\cos\varphi)} \tag{17}$$

with $E/mc^2 =: \varepsilon$ defines the angular intensity of the scattering process, as shown in Figure 2. To derive the compton spectrum in Figure 3, we have to map the angles φ to energies x

$$x = \frac{1}{1+\varepsilon(1-\cos\varphi)} \in [0, T_{\max}] \tag{18}$$

$$\Leftrightarrow \varphi = \arccos\left(1 - \frac{1-x}{x\varepsilon}\right) \tag{19}$$

The resulting spectrum neglects the peak broadening. Experimental data does not show this rather sharp Compton edge.

Another possibility is the occurrence of scattering outside the detector. The result is the so called backscatter peak at

$$E_{bs} = E_\gamma - T_{\max} \tag{20}$$

The cross section of Compton scattering is proportional to the number Z of electrons[4]

$$\sigma_C \propto \frac{Z}{E} \tag{21}$$

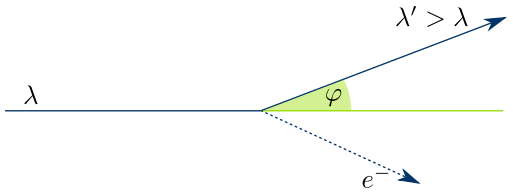

Figure 1. Geometry of Compton scattering of a photon with the wavelength λ before and λ' after the scattering detaching the electron e^-.

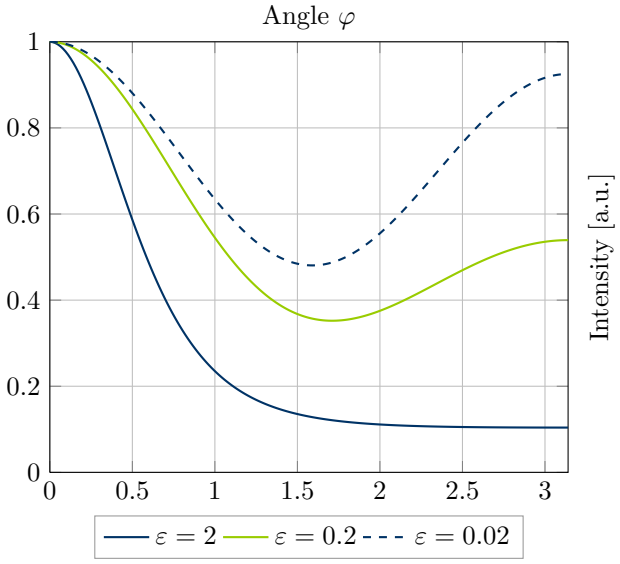

Figure 2. Angular distribution of the Compton spectrum[1]. This data is theoretical and neglects the peak broadening.

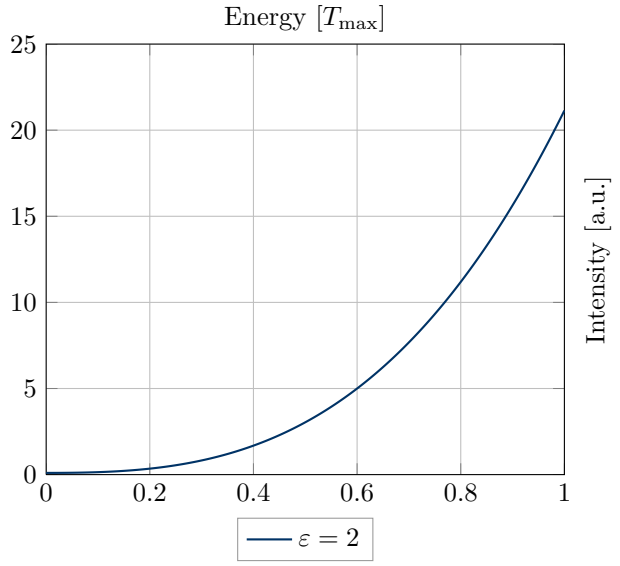

Figure 3. Energetic distribution [1, 3] of the Compton spectrum

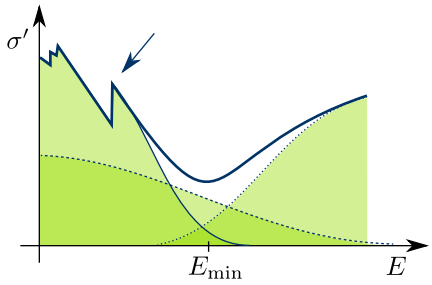

Figure 4. Dependence of σ' (stroked, bold) on the photon's energy according to [1, 4] with σ_P (stroked, thin), σ_C (dashed), σ_{PP} (dotted) and the K edge (arrow). $E_{\min}$ depends on the material used for the experiment and its typical value is about 5 MeV. Both the energy axis and the cross section acis are scaled logarithmically.

I.C Pair production

Another type of peaks are the escape peaks. In case the photon carries more than twice the rest energy of an electron, pair production is possible. The result of this process is one electron and one positron that will annihilate with another electron and emits two photons with the rest energy of an electron (511 keV). If one of these photons escapes the detector used for observing the experiment, the peak is called single-escape peak; if both photons escape the detector, it is called double-escape peak. For each photopeak E_x with an energy of more than 1022 keV, the escape peaks should occur at

$$E_s = E_x - m_e c^2 \qquad E_d = E_x - 2m_e c^2 \tag{22}$$

This process is possible outside the detector as well. In this case one of the photons can reach the detector which leads to an annihilation peak at

$$E_{an} = m_e c^2 \simeq 511 \text{ keV} \tag{23}$$

The corresponding cross section for pair production is[2]

$$\sigma_{PP} \propto Z^2 \ln E \tag{24}$$

The total cross section is given by

$$\sigma' = \sigma_P + \sigma_C + \sigma_{PP} \tag{25}$$

Figure 4 visualizes the different contributions.

I.D Setup

The most difficult yet promising part of this experiment was the setup's assembling and calibration. Figure 5 shows the wiring and causal dependencies of the experiment. We tried to use short cables in order to retain the signal quality. As the setup allows to define delays at several points, different cable lengths were not supposed to become an issue. Starting from the observed event, two scintillation detectors absorb the energy and produce a small signal. The following amplifiers create two signal pathways. The first one, issued directly after the signal from the detector arrives, is passed on to the single channel analyzer, whereas the second one, connected to a linear gate, is delayed by some microseconds. The amplifiers are responsible for turning the incoming peak into a pulse with a zero crossing. This part of the setup is identical for the photon and electron detection.

The following part of the setup is strictly necessary if coincident signals are the only ones to be captured. Otherwise, this part may be skipped and the output of the two linear gates may be directly connected to a multi channel analyzer. So far, the two detectors may register events or incoming radiation independent from each other. For radioactive events like the β^+ decay of ^{22}Na, it might be more interesting to assure that all incident radiation is caused by exactly one event. The main concept of the coincidence stage is to define a limit τ, so the multi channel analyzers only capture an event if the time lag of the two independent signals from the two detectors does not exceed τ. Therefore, the delay gate generators forward a rectangular pulse to the coincidence stage each time they receive an input from the single channel analyzers. Unlike the output of the linear gates, the amplitude of the rectangular pulse is not necessarily related to the radiation's energy, as checking for simultaneous detection is the only matter of particular interest. Shorter pulses lead to a higher demand in precision of signal path synchronisation and reduce the count rate for the multi channel analyzers. However, short pulses define a lower propability for random coincidence. Each device's delay should be adjusted in order to account for the different signal propagation delays. That way, the coincidence detector can be regarded as an AND gate triggering the

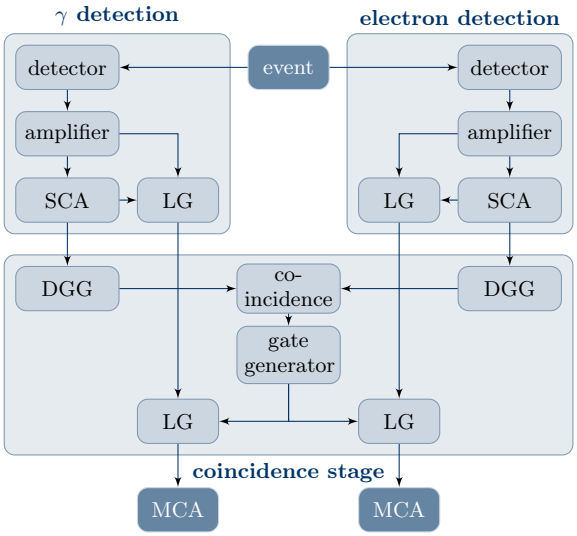

Figure 5. Block diagram containing the setup's wiring and causal dependencies. SCA and MCA denote single / muli channel analyzer, LG is an abbbreviation for a linear gate just like DGG is for a delayed gate generator.

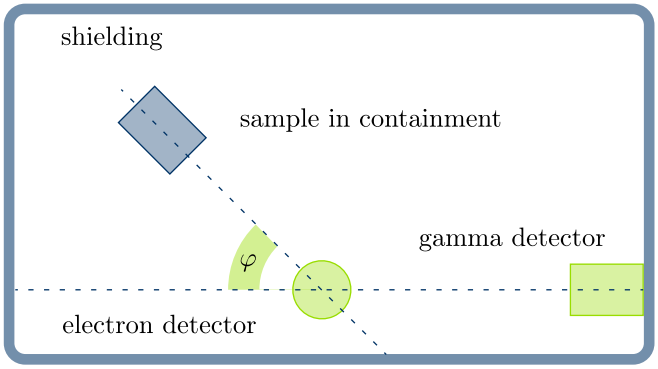

Figure 6. Setup for the measurement of dependencies on the angle φ. For all other measurements or calibration setups, the sample was placed between the electron detector and the gamma detector.

gate generator. The gate generator defines a time range τ'. Every signal reaching the linear gates of the coincidence stage during τ' will be recorded by the two multi channel analyzers.

For assembling, we started with observing the detectors' signal on an oscilloscope. Right behind the amplifier, we were able to register the delay between the two channels. The signal output of the single channel analyzer was quite unstable in amplitude, as we observed different radiation energies at that time, but the signal width remained more or less the same over time. The alternating amplitude is caused by the two relevant energies, the 511 keV annihilation line and the 1274 keV relaxation line of the ^{22}Na sample used for the calibration. As we set the oscilloscope's trigger on the zero crossing, the constant pulse width could easily be observed. We had some problems connecting the delayed gate generators to the coincidence detector as the signal was supposed to be inverted. When adjusting the single channel analyzers, the oscilloscope's output seemed to be invariant under changes of the settings for the lower and upper limit. Later on, it turned out that the window defined by these two knobs per single channel analyzer should be fully opened for all measurements with the exception of the angular dependencies. According to Table II, the photon detector is supposed to register two very close peaks for the 120° setting described in Figure 6 and the ^{22}Na sample. In order to distinguish the two close peaks, we narrowed the allowed energetic range for the electron detector's single channel analyzer to match only one pulse. The rather arbitrary limit was set to roughly 700 keV, thereby separating the two peaks at 1005 keV and 307 keV in the electron detector's spectrum. Distinguishing the two peaks in the photon detector would not be feasible. However, due to the coincidence stage, only events occurring in both detector pathways are kept for further analysis, so filtering the energies by adjusting only one single channel analyzer is sufficient.

Table II. Energies for Compton events for different radiations E and both the electron E_e and the photon E_γ.

angle [°]	E [keV]	E_e [keV]	E_γ [keV]
60	511	170	340
90	511	256	256
120	511	307	204
180	511	341	170
60	1274	707	567
90	1274	909	365
120	1274	1005	269
180	1274	1061	213

I.E Coincidence methods

In order to achieve less coarse measurements, a coincidence circuit is used. Basically, it only registers events in case the detectors register a photon and an electron at the same time or at least within a selectable time frame τ. Thus, a causal connection between the two events can be assumed as long as τ is small enough. Expecially, the energy of the electron and the one of the photon should sum up to the incoming radiation's energy.

As the 511 keV radiation of ^{22}Na is issued by β^+ decay and is subject to conservation of momentum, the particles are only emitted in pairs. Both the particles carry the same momentum but propagate in opposite directions. Therefore, placing the ^{22}Na sample right between the two detectors can be used for the calibration of the coincidence circuit. The 1274 keV line is due to the ground state relaxation of ^{22}Ne.

I.F Detector

The NaI scintillation counter consists of a crystal that is sensitive to photons with an energy of the radiation being analyzed and reacts with fluorescence to incoming photons. The resulting photons carry less energy than the first ones, but detach electrons from the side of the crystal that is covered by a photomultiplier due to photo effect. The other sides of the crystal are covered in order to reflect the radiation. The photomultiplier raises the current by a factor of 10^6 to 10^{10}, so even single photons can be detected. The resolution of this kind of detector is about 6-10% and the dead time in the order of 10^{-6}s[2, 5].

I.G Decays

There are three main types of decay. The most important of which in this experiment – see Table III – is the beta decay that follows

$$^1_0\mathrm{n} \rightarrow {}^1_1\mathrm{p} + \mathrm{e}^- + \overline{\nu}_e \tag{26}$$

for the β^- decay and

$$^1_1\mathrm{p} \rightarrow {}^1_0\mathrm{n} + \mathrm{e}^+ + \nu_e \tag{27}$$

Table III. Nuclides used in this experiment, their main decay type, the daughter nuclei and the most important photopeaks according to [6]

nuclide	decay	result	energy [keV]
$^{22}_{11}$Na	β^+	$^{22}_{10}$Ne (stable)	1274,5
$^{60}_{27}$Co	β^-	$^{60}_{28}$Ni (stable)	1173,2; 1332,5
$^{137}_{55}$Cs	β^-	$^{137}_{56}$Ba (stable)	661,7
$^{241}_{95}$Am	α	$^{237}_{93}$Np (α)	13,9; 59,5

for the β^+ decay. The daughter nuclei are mostly in an excited state. The positron resulting from β^+ decay annihilates within the detector or at least nearby so the intensity of the annihilation line is much higher than expected, especially since the annihilation leads to two 511 keV photons due to conservation of momentum.

The process of alpha decay can be described as

$$ {}^{A}_{Z}\mathrm{X} \rightarrow {}^{A-4}_{Z-2}\mathrm{Y} + {}^{4}_{2}\mathrm{He} \tag{28} $$

If the nucleus is in an excited state, it is possible that the energy difference to the ground state is directly emitted by an electron. This process is similar to the Auger process but involves only one electron.

$$ {}^{A}_{Z}\mathrm{X}^{*} \rightarrow {}^{A}_{Z}\mathrm{X} + \mathrm{e}^{-} \tag{29} $$

This effect is called internal conversion.

As most of the nuclides decay into stable ones, we can assume the radiation to be solely based on these nuclides. This even holds for ^{241}Am, as ^{237}Np has a half-life of about $2 \cdot 10^6$ years[6].

II Measurements

All peaks were expected to follow a Gaussian shape

$$ f(x) = a \exp\left(-\frac{(x-b)^2}{c^2}\right) \tag{30} $$

Fitting in general was performed using a nonlinear least-squares Marquardt-Levenberg implementation which calculates error estimates, as well.

II.A Background

For the first measurements, there was no need to focus on coincidence, so we switched the two linear gates of the coincidence state into the non-gated mode instead of changing the wiring. The coincidence filtering is only necessary to prove the conservation of energy and the conservation of momentum in the last measurements.

The settings for the two detectors have to be kept constant for the whole experiment, as changing anything would invalidate the calibration line. As Table III proves the 1.3 MeV line of ^{60}Co to have the highest energy of all lines to be observed during the experiment, we placed the ^{60}Co sample between the detectors and varied the high voltage for the two detectors. These voltages determine the amplitude of the voltages reaching the multi channel analyzers, that in turn discretize the signal voltage and omit peaks with a voltage exceeding the observed range. In order to observe the last line, we had to reduce the voltage for the electron detector.

Table IV. Duration of the measurements in seconds for both detectors. The slightly different times for the two detectors are due to manual operation. Measurements with ^{c} have been performed with an active coincidence stage.

measurement	γ [s]	e^- [s]
background	4753	4746
^{241}Am calibration	294	300
^{137}Cs calibration	430	437
^{60}Co calibration	1308	1317
^{22}Na spectrum	1308	1317
^{22}Na 60° compton^{c}	1217	1215
^{22}Na 90° compton^{c}	1319	1320
^{22}Na 120° compton^{c}	530	533
^{22}Na 120° compton^{c}: 0,5 MeV line	562	565
^{22}Na 120° compton^{c}: 1,3 MeV line	610	610

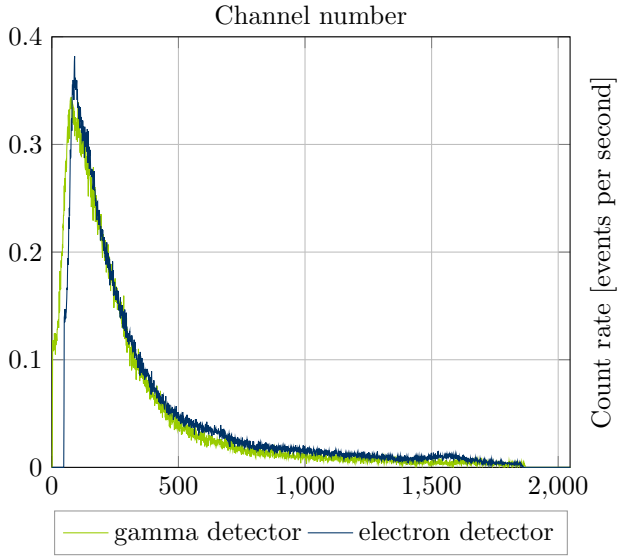

Figure 7. Background spectrum for both detectors. The gamma detector's counts have been scaled by a factor of 2.06 (see text).

For all experiments, with the exception of those with coincidence stage switched on, the background radiation has to be considered. As the count rate is rather low, we recorded the background radiation for both detectors for a long time. The duration of all datasets is shown in Table IV.

The most interesting result concerning the background radiation is the huge difference of the total count number for the two detectors. The gamma detector measured a count rate of 46,2 events per second, whereas the elec-

Table V. Position of the calibration peaks in terms of channel numbers for both the electron detector (e^-) and the gamma detector(γ).

sample	γ	e^-	energy [keV]
^{241}Am	(44 ± 1)	(68 ± 1)	59.5
^{137}Cs	(760 ± 1)	(741 ± 1)	661.7
^{60}Co	(1304 ± 3)	(1305 ± 3)	1173.2
^{60}Co	(1432 ± 4)	(1442 ± 2)	1332.5

tron detector registered 95,3 events per second. This is influenced by the shielding of the gamma detector as it is partial covered with lead. Bringing the total count rates into agreement by multiplying every data point from the gamma detector's background spectrum by 2.06, we get merly the same spectrum. The small but notable drift in Figure 7 is only an effect of the missing calibration.

II.B Calibration

For both detectors, the calibration line was derived from the spectra after subtracting the background spectrum with respect to the different recording times. The plain data is given in Table V and visualized in Figure 8. Starting from the channel number n, the energy can be calculated as follows

$$E(n) = \alpha x + \beta \tag{31}$$

Linear regression leads to

$$\alpha_\gamma = (0.87 \pm 0.03) \qquad \beta_\gamma = (15 \pm 20)$$

for the gamma detector and

$$\alpha_{e^-} = (0.91 \pm 0.02) \qquad \beta_{e^-} = (-7 \pm 10)$$

for the electron detector. Error propagation gives

$$\Delta E(n) = \sqrt{n^2(\Delta\alpha)^2 + (\Delta\beta)^2 + \alpha^2(\Delta n)^2} \tag{32}$$

Theoretically, the second peak of ^{241}Am could be used to add another data point to the fit. At least one half of the peak is visible. As the other half is missing, the determination of the peak's position is likely to introduce a rather big error. Therefore, we stuck to the peaks listed in the task description.

II.C Compton edges

So far, we used reference information concerning the peaks to analyze the direct relation between the channel number and the corresponding energy for both detectors. This information is necessary to do the inverse: derive energies from measured channel numbers.

Just to make sure that all relevant data has been recorded successfully, we captured the spectra for both detectors with the ^{22}Na sample. After removing the background radiation, the spectra were quite different. Figure 9 shows that the gamma detector got a complete spectrum whereas the electron detector was unable to record all peaks. This might be a result of the higher sensitivity of the gamma detector combined with the bigger dimensions of the gamma detector. Therefore, we primarily used the data from the gamma detector in order to determine the Compton edges for both the peaks.

The 511 keV peak itself is found at (503 ± 26) keV and the corresponding Compton edge is at (330 ± 22) keV. The 1274 keV line was found to be at (1236 ± 47) keV and the Compton edge was shifted to (1037 ± 41) keV. All these values agree with the reference data from Table II and Table III. Apparently, all measured values are slightly to low in terms of energy. The error determined by evaluating eqn. (32) is dominated by the uncertainty of the calibration line's zero crossing.

II.D Angular dependency

Up to this point, we have not used the coincidence stage. But in the last part of the experiment, we only got a spectrum for all angles alltogether. As mentioned above, the coincidence stage helps to reduce the total angular distribution to a narrow range of angles for each measurement. As this highly reduces the count rate, we used a ^{22}Na source with a higher intensity. As side effect, the background radiation has much less effect on the data.

Figures 10 and 11 show the results for the measurements with an active coincidence stage. For the gamma detector, the peaks' angular dependency is clearly visible. Table VI presents the resulting peak positions, as long as they are determinable. This is especially difficult for the $\varphi = 120°$ setting and the electron detector. Table II contains the estimate for the energies of scattered

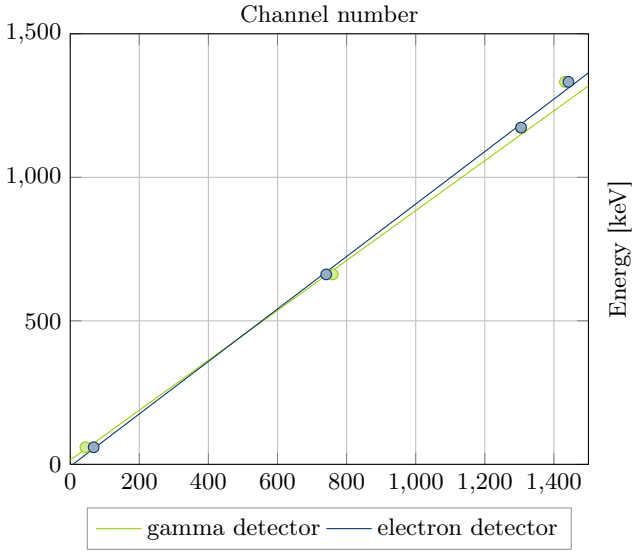

Figure 8. Calibration points with regression lines for both detectors. The errors are too small to be visible.

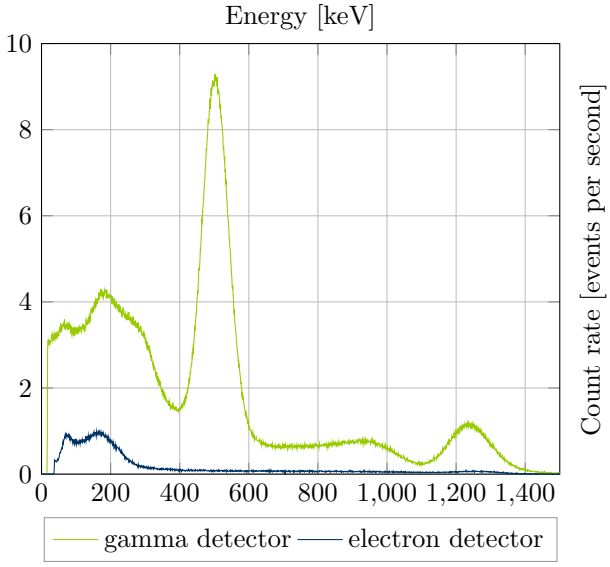

Figure 9. Spectra for determining the Compton edges for both detectors and the ^{22}Na sample after subtracting the background radiation. In order to keep the diagram legible, all error bars are omitted. The data was recorded while the coincidence stage was disabled.

Table VI. Position of the scattering peaks for different angles together with their original line energy for the two detector types. The error of the angle is estimated from the experimental setup. The three values marked with an asterisk are statistically comparable to the reference data. The other values are statistically equal to the reference data with the exception of those marked with a dash. For $\varphi = 120°$, the second line holds the numbers obtained by the separating settings for the single channel analyzer. The sums are espected to match the line energy due to energy conservation. All energies in keV.

angle [°]	line [keV]	e^- [keV]	γ [keV]	$\sum$ [keV]
(60 ± 5)	511	(150 ± 20)	(359 ± 23)	(509 ± 30)
(90 ± 5)	511	(222 ± 12)	(268 ± 22)	(490 ± 25)
(120 ± 5)	511	$^*(279 \pm 12)$	(214 ± 22)	(493 ± 25)
		$'(214 \pm 12)$	$'(276 \pm 22)$	(490 ± 25)
(60 ± 5)	1274	$^*(662 \pm 18)$	(558 ± 27)	$'(1220 \pm 32)$
(90 ± 5)	1274	$^*(888 \pm 22)$	(379 ± 23)	(1267 ± 32)
(120 ± 5)	1274	(949 ± 24)	(278 ± 22)	$'(1227 \pm 33)$
		(982 ± 23)	$^*(289 \pm 22)$	(1271 ± 32)

radiation for different angles and leads to the expectation of two peaks right next to each other in the electron detector's spectrum. As mentioned in the setup section, we recorded different spectra for a lowpass filter-like setup and for a highpass filter-like setup.

An in-depth inspection of the measured data reveals some strange deviations from the specified data format as the software that has been used for recording the multichannel analyzers' output seems to drop some channels on output. However, only some lines are missing so

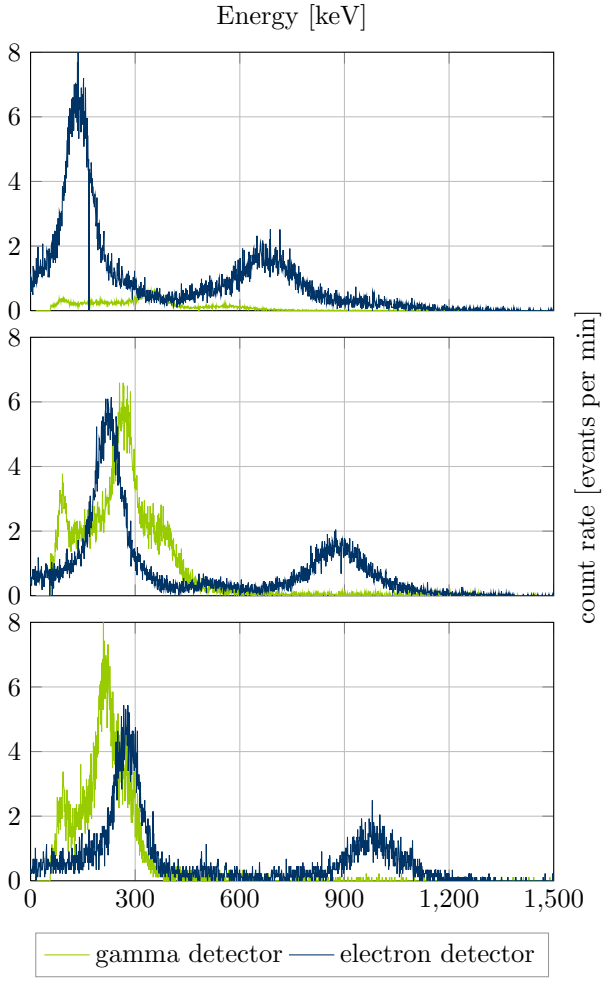

Figure 10. Spectra for the two detector types for three different angles: $\varphi = 60°$ is the topmost, $\varphi = 90°$ the intermediate and $\varphi = 120°$ the lowermost frame. All data was recorded with an active coincidence stage. Therefore, these diagrams are not comparable to the former spectra.

the analysis is not affected by this undocumented behavior. As for the gamma detector's spectra, the peaks' distance was not big enough to distinguish them safely for $\varphi = 120°$ in the initial setup. Nevertheless, fitting both peaks was possible in case the average value for both distributions has been kept constrained. This fitting was performed by a self-written computer program by rasterization of the quite small parameter range.

Figure 12 shows the final results. The experimental data confirms the theoretical model for the three acquired data points each. However these three points are not enough to prove the Compton formula, as especially the behavior for small angles is unclear by the sole analysis of the experimental data. Of course, using data from more angles can easily account for the gap as the experimental setup proved to give reasonable results.

The last column of Table VI presents the sum of the energies measured for each pair of gamma and electron

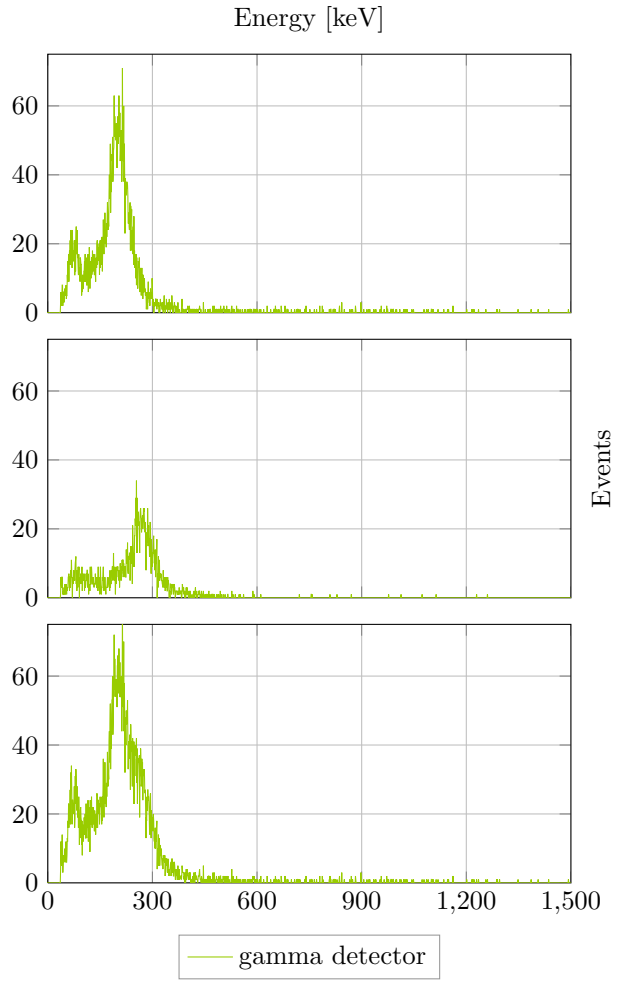

Figure 11. Spectra for the electron detector and $\varphi = 120°$. The topmost frame contains the data from the lowpass setup, the second frame presents the data from the highpass measurement and the lowermost frame contains the sum of the two other frames. All data was recorded with an active coincidence stage.

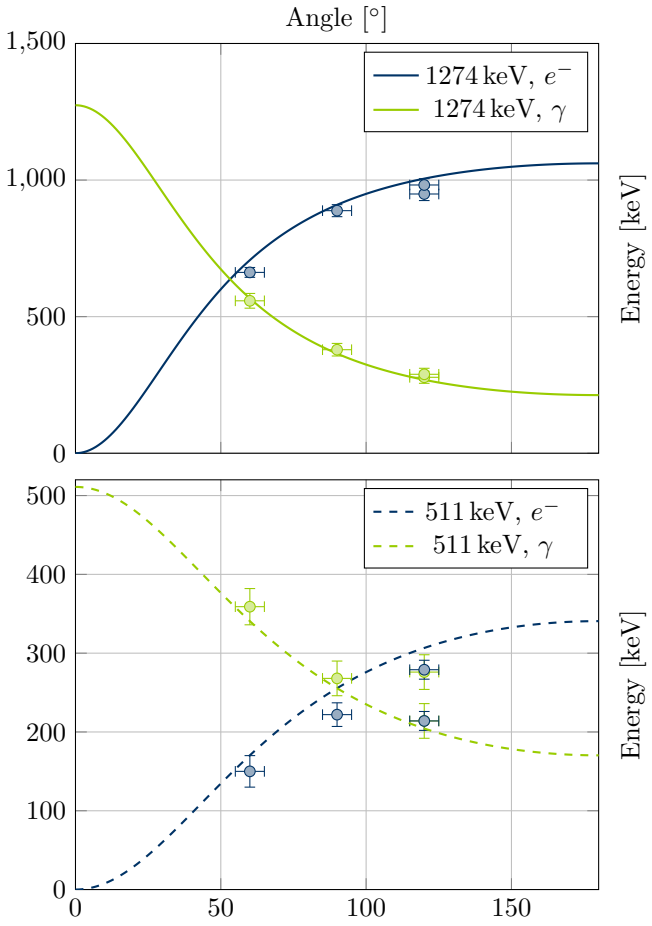

Figure 12. Final results for the dependency of the photons' and electrons' energy on the scattering angle. Each marker belongs to the nearest line of matching color.

peaks. The results are statistically equal to the expected values, the energy of the corresponding lines. There are only two exceptions: the $\varphi = 120°$ measurements without the energy line separation by adhusting the single channel analyzer window.

III Discussion

Based on the knowledge about the setup from the detailled step-by-step analysis of the signal, we were able to use the coincidence stage in order to obtain better and more accurate results for the angular dependency of the Compton scattering. Starting from the background radiation and simple spectra, we first calibrated the multi-channel analyzers and went on to measure the Compton edges. All the values obtained by this part of the experiment agreed with the calculated reference data. Afterwards, the angular dependency of the electrons' and photons' energies turned out to match the theoretical expectations for the measured data points. It might be necessary to test for the peaks' positions for even smaller angles in order to prove the Compton relation.

When interpreting the last diagram in Figure 12, one has to keep in mind that the angular error increases the uncertainty of the energy by some 10 keV, as well. This dependency is not included in the energy error bars, so they appear to small.

The biggest problem of the analysis is the calibration error. The linear regression for the calibration lines tends to result in rather small errors for the slope but in comparably big errors for the zero crossing. As the zero crossing value defines a constant offset, this introduces a systematic error for all of the results. This error is not neglectable, because ten channels map to some 9 keV. Adding further calibration peaks or by switching to semiconductor detectors might help. Their resolution in terms of $\Delta E/E$ is much better than the one of the scintillation detectors used in this experiment.

As final observation, the total count rate of the two detectors with an active coincidence stage does sum up

to approximately the same value (the biggest relative difference is about 0.36%), whereas the relative difference in the total count rates may exceed 100% without the coincidence stage. Therefore, using a sample with a smaller activity is not necessary, although in theory this would lead to better results due to less random coincidence. The same argument holds for the coincidence time window.

[1] W. R. Leo, *Techniques for Nuclear and Particle Physics Experiments* (Springer).

[2] R. S. P. Marmier, E. Sheldon, *Kernphysik I* (Verlag der Fachvereine an der ETH Zürich, 1973).

[3] B. W. K. Bethge, G. Walter, *Kernphysik: Eine Einführung* (Springer, 2008).

[4] W. Demtröder, *Experimentalphysik 4: Kern-, Teilchen- Und Astrophysik* (Springer, 2010).

[5] T. Friese, *Skript zur Vorlesung Nukleare Elektronik*.

[6] National Nuclear Data Center, "Nudat 2.6," http://www.nndc.bnl.gov/nudat2/ (2012).